Microchimica Acta (2019) 186: 202
https://doi.org/10.1007/s00604-019-3303-2

ORIGINAL PAPER

Fluorometric determination of the activity of alkaline phosphatase and its inhibitors based on ascorbic acid-induced aggregation of carbon dots

Pengjuan Ni[1] · Junfeng Xie[2] · Chuanxia Chen[1] · Yuanyuan Jiang[1] · Yizhong Lu[1] · Xun Hu[1]

Received: 9 November 2018 / Accepted: 3 February 2019 / Published online: 22 February 2019

Abstract

The authors describe a fluorometric method for determination of the activity of alkaline phosphatase (ALP) and its inhibitors. Nitrogen and boron co-doped carbon dots (C-dots) with excitation/emission peaks at 490/540 nm act as the fluorescent probe. The C-dots were prepared by hydrothermal carbonization starting from 3-aminophenylboronic acid as the sole precursor. On the basis of the boronic acid-triggered specific reaction with *cis*-diols, the boronic acid modified C-dots can bind to ascorbic acid that is generated by ALP-catalyzed hydrolysis of ascorbic acid 2-phosphate. This results in particle aggregation and quenching of fluorescence. If the ALP inhibitor Na_3VO_4 is introduced into the system, the activity of ALP is reduced and the fluorescence of C-dots recovers. This fluorometric method allows for the determination of ALP activity in the range from 0.2 to 6.0 mU mL^{-1} with a detection limit of 0.16 mU mL^{-1}. The IC_{50} value for the inhibitor Na_3VO_4 is 3.6 μM. The method is convenient and cost-effective. It does not require complicated operations and in our perception widens the scope of applications of C-dots in bioanalytical sciences.

Keywords Enzyme inhibition · Sodium orthovanadate · Fluorometry · Ascorbic acid · Ascorbic acid 2-phosphate · *cis*-Diols · 3-Aminophenylboronic acid

Introduction

Alkaline phosphatase (ALP) is a critical enzyme in phosphate metabolism due to its ability to catalyze the hydrolysis of phosphoryl esters [1–3]. Moreover, ALP is commonly used as an important biomarker for clinical diagnosis since its abnormal levels is closely associated with many diseases such as bone diseases, diabetes, prostatic cancer and liver dysfunction [4]. Therefore, it is of great importance to develop a sensitive and selective method for ALP detection.

Fluorimety exhibits the advantages of high sensitivity, rapid response and easy operation [5–9], which shows great potential for ALP activity detection [10–12]. A number of fluorescent methods for ALP activity detection have been reported by utilization of organic fluorescent probes [13, 14], semiconductor quantum dots [15], fluorescent polymers [16] and noble metal nanoclusters [17, 18]. The poor water solubility for the organic probes, high toxicity for semiconductor quantum dots, laborious and complex synthesis procedure for fluorescent polymers, high cost and poor stability for noble metal nanoclusters have undoubtedly limited their further practical applications [19]. Consequently, it is still challenging to develop a fluorescent probe for ALP activity detection, especially the fluorescent probe shows the advantages of good water solubility, low toxicity, simple synthesis procedures, cost-effectiveness and high stability.

Electronic supplementary material The online version of this article (https://doi.org/10.1007/s00604-019-3303-2) contains supplementary material, which is available to authorized users.

✉ Pengjuan Ni
mse_nipj@ujn.edu.cn

✉ Yizhong Lu
mse_luyz@ujn.edu.cn

✉ Xun Hu
Xun.Hu@outlook.com

[1] School of Materials Science and Engineering, University of Jinan, Jinan 250022, People's Republic of China

[2] College of Chemistry, Chemical Engineering and Materials Science, Key Laboratory of Molecular and Nano Probes (Ministry of Education), Collaborative Innovation Center of Functionalized Probes for Chemical Imaging in Universities of Shandong, Institute of Molecular and Nano Science, Shandong Normal Univeristy, Jinan, Shandong 250014, People's Republic of China

Carbon quantum dots (C-dots), a new class of carbon nanoparticles with size less than 10 nm, have drawn increasing research attentions due to their outstanding advantages [20]. As a consequent, C-dots have been widely used in many fields, such as photocatalysis [21, 22], biological imaging [23, 24], biosensing [25, 26], photovoltaic device [27, 28] and drug/gene delivery [29, 30]. However, the fluorescent assays based on C-dots for ALP activity detection have been rarely reported. Qian et al have proposed a novel fluorescent method for sensitive detection of ALP activity based on the C-dots-Cu^{2+}- pyrophosphate ion (PPi) system [31]. The C-dots were prepared by concentrated acid treatment method, which was dangerous and not environmental-friendly. Qu et al reported a fluorescent assay for ALP activity detection based on C-dots-MnO_2 nanosheets [32]. Though this assay showed high sensitivity and selectivity, it was limited by the complex and time-consuming procedures for the preparation of MnO_2 nanosheets. Tang et al reported a fluorescent assay for ALP activity detection by utilization of the β-cyclodextrin-modified C-dots through host-guest recognition. But it showed the disadvantage of complex process of the surface modification for C-dots. Therefore, it irradiates us to develop facile, sensitive and selective method for ALP activity detection using functionalized C-dots with simple and environmental-friendly preparation method.

In this paper, we present a convenient and highly sensitive fluorescent assay for ALP activity and its inhibitor detection by using boron and nitrogen co-doped C-dots as fluorescent probe. The C-dots were easily prepared by utilization of 3-aminophenylboronic acid (ABPA) as the sole precursor thorough one-step hydrothermal method [33]. The C-dots are rich in boronic acids group, which are reactive to *cis*-diols structure and can covalently bind with the ascorbic acid (AA) obtained from the hydrolysis of ascorbic acid 2-phosphate (2-AAP) by ALP. This results in aggregation and fluorescence quenching of C-dots. The introduction of ALP inhibitor can inhibit the generation of AA to achieve the fluorescence recovery. Therefore, the C-dots can be employed to fabricate a sensitive and selective fluorescence assay for ALP activity and its inhibitor detection.

Experimental

Reagents and apparatus

ABPA, diethanolamine (DEA), bovine serum albumin (BSA), trypsin and magnesium chloride hexahydrate ($MgCl_2$•$6H_2O$) were bought from Aladdin Reagent Company (Shanghai, China, www.aladdin-e.com). Lysozyme, pepsin and pancreatin were purchased from Shanghai Macklin Biochemical Co., Ltd. (Shanghai, China, www.macklin.cn). Glucose oxidase (GOx) was supplied by Sangon Biotech Co., Ltd. (Shanghai, China, www.sangon.com). Glucose (Glu), dopamine (DA), ALP, 2-

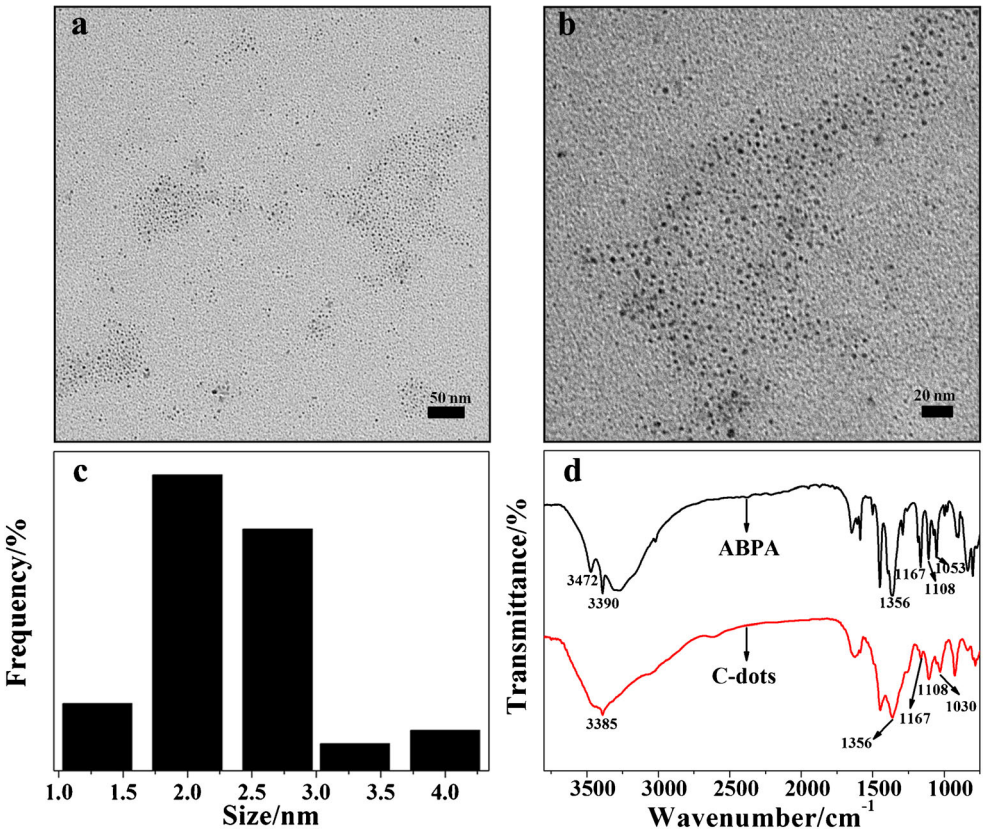

Fig. 1 TEM images of C-dots taken at low (**a**) and high magnifications (**b**). **c** Size distribution of the C-dots (collected from 100 particles). **d** FT-IR spectra of the ABPA and the C-dots

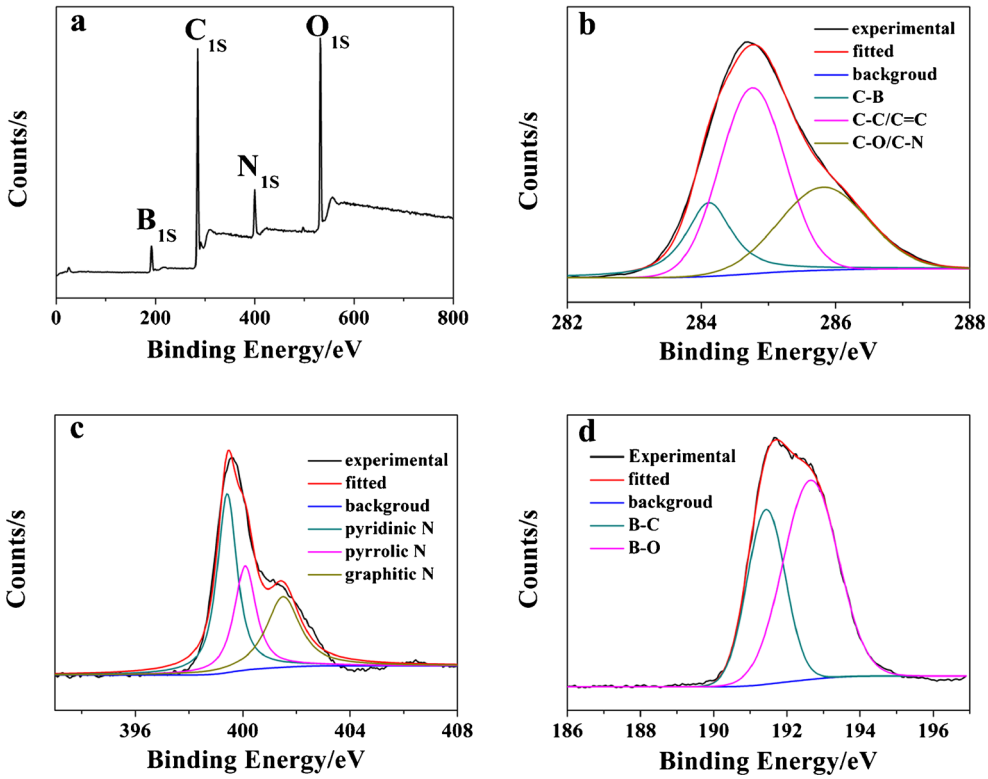

Fig. 2 **a** Entire XPS scanning spectrum of C-dots. The XPS high-resolution survey scan of C1s (**b**), N1 s (**c**) and B1s (**d**) of the C-dots

AAP and AA were acquired form Sigma-Aldrich (St. Louis, USA, www.sigmaaldrich.com).

Fluorescence spectra were recorded on a RF-6000 spectrofluorometer (Shimadzu, Japan, www. shimadzu.com.cn). The fluorescence emission spectra were collected in the wavelength range from 510 nm to 620 nm at the excitation wavelength of 490 nm. The excitation and emission slits were set as 5.0 nm and 15.0 nm, respectively. Transmission electron microscopy (TEM) images were obtained on JEM-1400 (JEOL Ltd., Japan, www.jeol.co.jp). X-ray photoelectron spectra (XPS) were performed with an ESCALAB 250Xi spectrometer (Thermo Fisher Scientific, USA, www.thermo.com). Fourier-transform infrared (FT-IR) spectra were recorded on a Nicolet 380 FT-IR spectrophotometer (Thermo Fisher Scientific, USA, www. thermo.com).

ALP activity and Na_3VO_4 detection

For ALP activity detection, 380 μL of DEA buffer (1 M, pH 9.8), 10 μL of 50 mM $MgCl_2$, 100 μL of 40 mM 2-AAP, 10 μL of ALP with various enzyme activities, 10 μL of C-dots and 490 μL of ultrapure water were successively added into a 1.5 mL calibrated test tube. The solutions were mixed thoroughly and incubated at 37 °C for 2 h. Finally, it was transferred for fluorescence spectra measurements.

Na_3VO_4 is used as a model to study the potential application of this fluorescent assay for ALP inhibitor screening. In detail, 370 μL of DEA buffer (pH 9.8), 10 μL of 50 mM $MgCl_2$, 10 μL of 3 U mL^{-1} ALP and 10 μL of different amounts of Na_3VO_4 were firstly added in 1.5 mL calibrated test tube and incubated for 30 min at 37 °C. Subsequently,

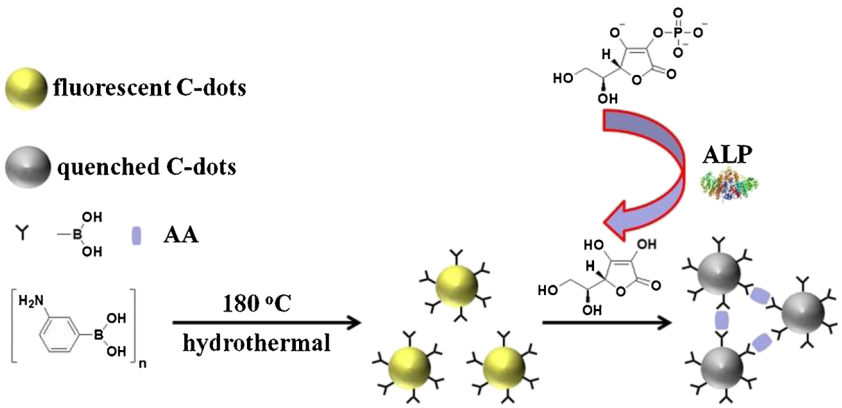

Scheme 1 Schematic illustration of synthesis of C-dots and the working principle for ALP activity detection

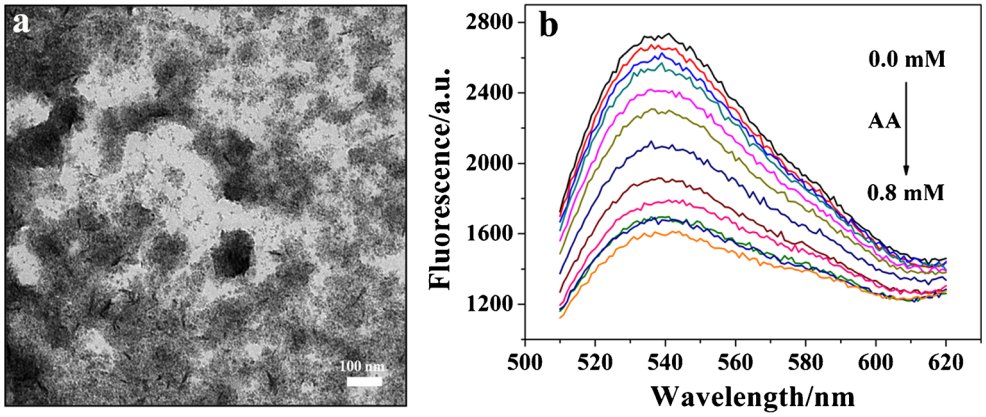

Fig. 3 **a** TEM images of the C-dots after the addition of AA. **b** Fluorescence spectra of the C-dots before and after the introduction of different concentrations of AA. From top to down, the concentrations of AA are 0.0, 0.05, 0.1, 0.15, 0.2, 0.25, 0.3, 0.35, 0.4, 0.45, 0.5 and 0.8 mM. Detection conditions: 10 μL C-dots, 4 mM 2-AAP, 0.5 mM $MgCl_2$, excitation/emission peaks at 490/540 nm

100 μL of 40 mM 2-AAP and 10 μL of C-dots were added and diluted to 1 mL with ultrapure water. Finally, the above solutions were incubated at 37 °C for another 2 h before the fluorescence spectra measurements.

Detection ALP in real samples

For detection ALP in diluted human serum samples, 380 μL of DEA buffer (pH 9.8), 10 μL of 50 mM $MgCl_2$, 100 μL of 40 mM 2-AAP, 10 μL of ALP with various activities prepared by 10% human serum samples, 10 μL of the C-dots and 490 μL of ultrapure water were mixed thoroughly and incubated at 37 °C for 2 h before the fluorescence spectra measurements.

Results and discussions

Characterization of the C-dots

The morphologies of the C-dots characterized by TEM are displayed in Fig. 1a and b. The C-dots are mono-dispersed and show a size distribution ranging from 1.3 to 4.0 nm with an average diameter of 2.4 nm (Fig. 1c). The surface composition of the C-dots is confirmed by using FT-IR. As shown in Fig. 1d, the peak at 3385 cm^{-1} in the FT-IR curve of C-dots is assigned to the stretching vibration of N-H, corresponding to the peaks at 3472 and 3390 cm^{-1} of the ABPA. In addition, the asymmetric stretching vibration of B-O at 1356 cm^{-1}, the bending vibration of B-O-H at 1167 cm^{-1}, C-B stretching vibration at 1108 cm^{-1} and B-O-H deformation vibration at 1030 cm^{-1} are also observed in the FT-IR of C-dots [34]. Furthermore, the composition of the C-dots is characterized by XPS. As shown in Fig. 2a, the survey spectra of the synthesized C-dots implies the presence of C, N, O as well as B elements. The high-resolution spectrum of C1s reveals the presence of C-B (284.1 eV), C-C/C=C (284.8 eV) and C-O/C-N (285.8) on the surface of C-dots (Fig. 2b). The N1 s spectrum can be deconvoluted into three peaks centered at 399.4, 400.1 and 401.5 eV, corresponding to pyridinic N, pyrrolic N and graphitic N (Fig. 2c). From the high-resolution B1s spectrum (Fig. 2d), the two peaks at 191.4 and 192.7 eV are attributed to B-C and B-O, respectively. These results reveal that B and N have been successfully doped in

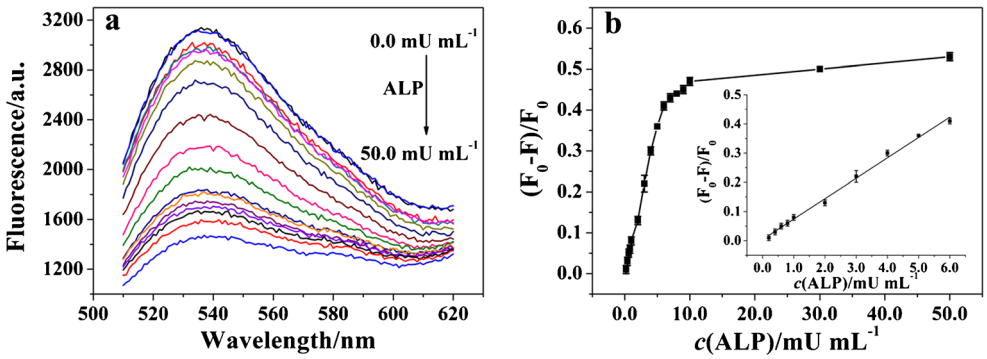

Fig. 4 **a** The fluorescence spectra of C-dots before and after the addition of various activities of ALP. From top to down, the activities of ALP are 0.0, 0.2, 0.4, 0.6, 0.8, 1.0, 2.0, 3.0, 4.0, 5.0, 6.0, 7.0, 8.0, 9.0, 10.0, 30.0 and 50.0 mU mL^{-1}. **b** The relationship between the $(F_0\text{-}F)/F_0$ and ALP activity. Inset shows the linear plot of the $(F_0\text{-}F)/F_0$ as a function of ALP activity. F_0 and F are the fluorescence intensity of the detection system in the absence and presence of ALP, respectively. Conditions: 10 μL C-dots, 4 mM 2-AAP and 0.5 mM $MgCl_2$, excitation/emission peaks at 490/540 nm. Error bars represent the standard deviation of three individual measurements

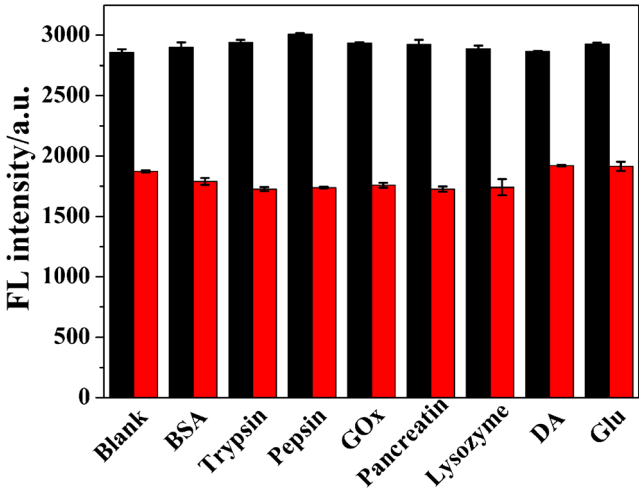

Fig. 5 The fluorescence intensity of the detection solution after the addition of possible interferences without (black) or with ALP (red). All the concentrations of these possible interfering substances and ALP are 0.5 μg mL^{-1}. The detection conditions for the selectivity test are the same as that for ALP detection except that the ALP is replaced by the possible interference or ALP and interference are simultaneously introduced. Error bars demonstrate the standard deviation of three independent measurements

the C-dots and the C-dots are functionalized with boronic acid group. The quantum yield (QY) of C-dots is calculated to be 15.4% % using Rhodamine B in ethanol solution as the standard (detailed information for the measurement of QY are shown in the electronic supporting material).

Principle of the detection method

The distinguished properties of C-dots make them possible to detect various important targets. Herein, a novel fluorescent assay for sensitive detection of ALP activity has been proposed thorough the boronic acid-modified C-dots. As shown in Fig. S1, the C-dots show largest emission intensity at 540 nm when excited at 490 nm. When either 2-AAP or ALP is introduced, the emission intensity of C-dots keep almost unchanged. However, when 2-AAP and ALP are simultaneously added, the emission intensity of C-dots decrease obviously. Therefore, it proves that it is AA generating from the hydrolysis of 2-AAP by ALP that causes the fluorescence quench of C-dots. According to the above experimental results and previous reports that the boronic acids can bind with *cis*-diols to form stable boronate complexes [35], a possible detection mechanism is proposed (Scheme 1). As shown in Fig. 3a, the initial dispersed C-dots aggregates after the incubation with AA. At the same time, the fluorescence of C-dots decreases gradually with the increasing concentration of AA (Fig. 3b). Consequently, it may be the aggregation of C-dots result in the fluorescence quench. The Fig. S2 shows there is no overlap between the absorption spectrum AA and the excitation or emission spectra of C-dots. Therefore, the fluorescence resonance energy transfer and inner filter effect based mechanisms can be excluded. Based on a previous report [36], the fluorescence quench of C-dots may be due to the surface quenching states induced mechanism.

Optimization of the detection conditions

To obtain better detection performances, several experimental conditions including the concentration of 2-AAP, the volume of C-dots and incubation time are optimized. We utilize $(F_0\text{-}F)/F_0$ as the criterion to optimize the experimental conditions, where F_0 and F are the fluorescence intensity of C-dots at 540 nm in the absence and presence of ALP, respectively. The optimum detection conditions should be as follows: (a) the concentration of 2-AAP is 4.0 mM (Fig. S3), (b) the volume of C-dots is 10 μL (Fig. S4), (c) the incubation time is 120 min (Fig. S5).

Analytical performances for ALP screening

Under the optimal detection conditions, the sensitivity for ALP activity detection is carefully studied. Figure 4a shows the fluorescence spectra of the detection system upon the introduction of various activities of ALP ranging from 0.0 to 50.0 mU mL^{-1}. As the activity of ALP increase, the concentration of AA generated by the ALP-catalyzed hydrolysis of 2-AAP increases within certain activity range. As a consequent, the fluorescence intensity of C-dots decreases gradually. While, the $(F_0\text{-}F)/F_0$ increases systematically and

Table 1 Recovery analysis of ALP activity in serum samples

Sample	Amount added (mU mL^{-1})	Amount found[a] (mU mL^{-1})	Recovery (%)	RSD (%)
1	2.0	2.21 ± 0.18	110	8.14
	3.0	2.95 ± 0.12	98.3	4.07
2	2.0	1.95 ± 0.09	97.5	4.61
	3.0	2.95 ± 0.18	98.3	6.10
3	0.5	0.58 ± 0.05	116	8.62
	1.0	1.07 ± 0.02	107	1.87

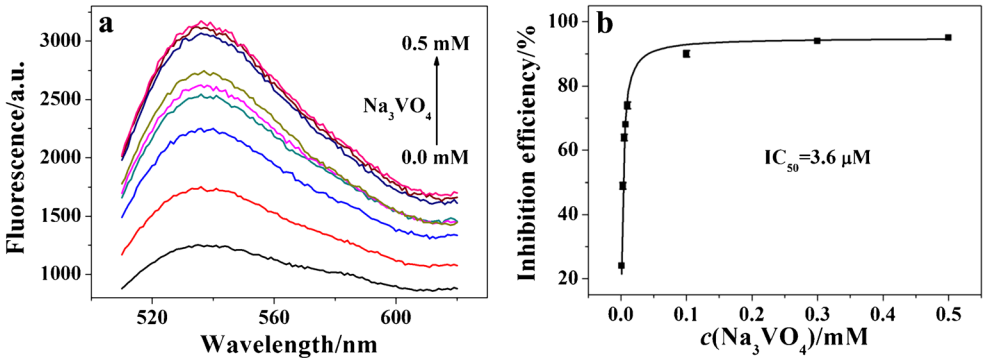

Fig. 6 **a** Fluorescence spectra of C-dots in the presence of 2-AAP (4.0 mM), ALP (30.0 mU mL^{-1}) and different concentrations of Na_3VO_4. From down to top the concentrations of Na_3VO_4 are 0.0, 1.0, 3.0, 5.0, 7.0, 10.0 μM, 0.1, 0.3 and 0.5 mM. **b** The plot of the IE of Na_3VO_4 to ALP versus the concentration of Na_3VO_4. Error bars are the standard deviation of three independent measurements

reaches a plateau when the activity of ALP exceeds 10.0 mU mL^{-1} (Fig. 4b). A good linear behavior between the $(F_0\text{-}F)/F_0$ and ALP activity in the range from 0.2 to 6.0 mU mL^{-1} is obtained. The linear equation is $(F_0\text{-}F)/F_0 = 0.004 + 0.070c_{ALP}$ (mU mL^{-1}), with a correlation coefficient of 0.994. The detection limit is estimated to be 0.16 mU mL^{-1} based on signal-to-noise ratio of 3. Moreover, we compare the analytical performances of this method with other methods for ALP activity detection reported elsewhere. As shown in the Table S1, the detection sensitivity is comparable or even higher than other methods. Additionally, though this method needs longer detection time, it is more convenient by just mixing C-dots, 2-AAP, ALP and buffer together. The repeatability of this assay is evaluated by six repeated measurements of 3.0 mU mL^{-1} ALP, and the relative standard deviation (RSD) is calculated to be 2.0%, indicating the reliability of this assay.

To validate the specificity of the assay for ALP activity detection, the effects of BSA, trypsin, pepsin, GOx, pancreatin, lysozyme, DA and Glu are explored. Under the same detection conditions, only these interferences added simultaneously with ALP can significantly induce the decrease of the fluorescence intensity, whereas no obvious fluorescence intensity change is found after the addition of these possible interferences without the ALP (Fig. 5). Therefore, this assay shows high selectivity o for ALP detection.

To demonstrate the practical use of this assay, we attempt to detect ALP in diluted human serum samples (10%). ALP with activities of 0.5, 1.0, 2.0 and 3.0 mU mL^{-1} are added and detected by this assay. As presented in Table 1, the recoveries are in the range from 97.50% to 116% with RSD ranging from 1.87% to 8.62%. The good recoveries and acceptable RSD has definitely demonstrate that this assay has been successfully employed for ALP activity detection in biological samples.

ALP inhibitor screening

As the overexpression of ALP is associated with several diseases, therefore, potent inhibitors of ALP may be used as therapeutic agents [37]. Therefore, this convenient assay enables us to study its potential application in ALP inhibitor screening. Na_3VO_4, a well-known inhibitor for ALP, is used as a model to evaluate the inhibitory effect. The ability of ALP to catalyze the hydrolysis of 2-AAP is very much weakened with the increasing concentrations of Na_3VO_4 and a relative low concentration of AA is released. As a result, the fluorescence intensity of C-dots increases gradually (Fig. 6a). The inhibition efficiency (IE) is calculated by the following eq. $IE(\%) = 100 \times (F_i\text{-}F)/(F_0\text{-}F)$, where F_i represents the fluorescence intensity of the C-dots after the addition of 2-AAP, ALP and Na_3VO_4. The IE of Na_3VO_4 is evaluated by IC_{50} value, which is the concentration of Na_3VO_4 needed for 50% inhibition of ALP activity. From the plot of IE versus Na_3VO_4 concentration (Fig. 6b), the IC_{50} value is calculated to be 3.6 μM. The results undoubtedly indicate that this fluorescence assay can be used for the screening of ALP inhibitors.

Conclusions

Based on the fact that AA can lead to the aggregation of the boronic acid-modified C-dots, a novel fluorometric method for ALP activity and its inhibitor screening has been developed. ALP is able to catalyze the hydrolysis 2-AAP to obtain AA, resulting in the fluorescence quench of C-dots. While the fluorescence recovers after the introduction of Na_3VO_4 since the ALP activity is inhibited. Though this method needs longer detection time, it shows several distinctive merits. Firstly, the C-dots are easily prepared and they possess good water solubility. Secondly, the detection procedures for ALP and its inhibitor is convenient by just mixing C-dots, ALP, 2-AAP and buffer together. Finally, this method shows high sensitivity and good selectivity. Moreover, this method may be not only used for ALP activity and its inhibitor detection, but also make a great contribution to the development of bioassays based on the C-dots.

Acknowledgments This work was financially supported by the National Natural Science Foundation of China (21705056), the program for Young Taishan Scholars of Shandong Province, the Natural Science Foundation of Shandong Province (ZR2017MB022, ZR2018BB057 and ZR2018PB009) and the start-up funding from University of Jinan (511-1009408, 511-1009424).

Compliance with ethical standards The author(s) declare that they have no competing interests.

References

1. Kang EB, Choi CA, Mazrad ZAI, Kim SH, In I, Park SY (2017) Determination of Cancer cell-based pH-sensitive fluorescent carbon nanoparticles of cross-linked polydopamine by fluorescence sensing of alkaline phosphatase activity on coated surfaces and aqueous solution. Anal Chem 89:13508–13517
2. Li SJ, Li CY, Li YF, Fei J, Wu P, Yang B, Ou-Yang J, Nie SX (2017) Facile and sensitive near-infrared fluorescence probe for the detection of endogenous alkaline phosphatase activity in vivo. Anal Chem 89:6854–6860
3. Tang ZW, Zhang HF, Ma CB, Gu P, Zhang GH, Wu KF, Chen MJ, Wang KM (2018) Colorimetric determination of the activity of alkaline phosphatase based on the use of cu(II)-modulated G-quadruplex-based DNAzymes. Microchim Acta 185:109
4. Zhao JH, Wang S, Lu SS, Bao XF, Sun J, Yang XR (2018) An enzyme cascade-triggered fluorogenic and chromogenic reaction applied in enzyme activity assay and immunoassay. Anal Chem 90:7754–7760
5. Zhang N, Si YM, Sun ZZ, Chen LJ, Li R, Qiao YC, Wang H (2014) Rapid, selective, and ultrasensitive fluorimetric analysis of mercury and copper levels in blood using bimetallic gold-silver nanoclusters with "silver effect"-enhanced red fluorescence. Anal Chem 86: 11714–11721
6. Cai YY, Feng LP, Hua Y, Liu H, Yin MY, Lv XX, Li S, Wang H (2018) Q-graphene-loaded metal organic framework nanocomposites with water-triggered fluorescence turn-on: fluorimetric test strips for directly sensing trace water in organic solvents. Chem Commun 54:13595–13598
7. Fan C, Lv XX, Liu FJ, Feng LP, Liu M, Cai YY, Liu H, Wang JY, Yang YL, Wang H (2018) Silver nanoclusters encapsulated into metal-organic frameworks with enhanced fluorescence and specific ion accumulation toward the microdot array-based fluorimetric analysis of copper in blood. ACS Sens 3:441–450
8. Feng LP, Sun ZZ, Liu H, Liu M, Jiang Y, Fan C, Cai YY, Zhang S, Xu JH, Wang H (2017) Silver nanoclusters with enhanced fluorescence and specific ion recognition capability triggered by alcohol solvents: a highly selective fluorimetric strategy for detecting iodide ions in urine. Chem Commun 53:9466–9469
9. Feng LP, Liu M, Liu H, Fan C, Cai YY, Chen LJ, Zhao ML, Chu S, Wang H (2018) High-throughput and sensitive fluorimetric strategy for microRNAs in blood using wettable microwells array and silver nanoclusters with red fluorescence enhanced by metal organic frameworks. ACS Appl Mater Interfaces 10:23647–23656
10. Wang HB, Li Y, Chen Y, Zhang ZP, Gan T, Liu YM (2018) Determination of the activity of alkaline phosphatase by using nanoclusters composed of flower-like cobalt oxyhydroxide and copper nanoclusters as fluorescent probes. Microchim Acta 185: 102
11. Xu AZ, Zhang L, Zeng HH, Liang RP, Qiu JD (2018) Fluorometric determination of the activity of alkaline phosphatase based on the competitive binding of gold nanoparticles and pyrophosphate to $CePO_4$:Tb nanorods. Microchim Acta 185:288
12. Xue Q, Cao XY, Zhang CL, Xian YZ (2018) Polydopamine nanodots are viable probes for fluorometric determination of the activity of alkaline phosphatase via the in situ regulation of a redox reaction triggered by the enzyme. Microchim Acta 185:231
13. Zhang HT, Xiao P, Wong YT, Shen W, Chhabra M, Peltier R, Jiang Y, He YT, He J, Tan Y, Xie YS, Ho D, Lam YW, Sun JP, Sun HY (2017) Construction of an alkaline phosphatase-specific two-photon probe and its imaging application in living cells and tissues. Biomaterials 140:220–229
14. Gao ZW, Sun JY, Gao M, Yu FB, Chen LX, Chen QG (2018) A unique off-on near-infrared cyanine-based probe for imaging of endogenous alkaline phosphatase activity in cells and in vivo. Sensors Actuators B Chem 265:565–574
15. Liu SY, Wang XY, Pang S, Na WD, Yan X, Su XG (2014) Fluorescence detection of adenosine-5′-triphosphate and alkaline phosphatase based on the generation of CdS quantum dots. Anal Chim Acta 827:103–110
16. Sun JY, Mei H, Gao F (2017) Ratiometric detection of copper ions and alkaline phosphatase activity based on semiconducting polymer dots assembled with rhodamine B hydrazide. Biosens Bioelectron 91:70–75
17. Liu HJ, Li M, Xia YN, Ren XQ (2017) A turn-on fluorescent sensor for selective and sensitive detection of alkaline phosphatase activity with gold nanoclusters based on inner filter effect. ACS Appl Mater Interfaces 9:120–126
18. Halawa MI, Gao WY, Saqib M, Kitte SA, Wu FX, Xu GB (2017) Sensitive detection of alkaline phosphatase by switching on gold nanoclusters fluorescence quenched by pyridoxal phosphate. Biosens Bioelectron 95:8–14
19. Xiao T, Sun J, Zhao JH, Wang S, Liu GY, Yang XR (2018) FRET effect between fluorescent polydopamine nanoparticles and MnO_2 nanosheets and its application for sensitive sensing of alkaline phosphatase. ACS Appl Mater Interfaces 10:6560–6569
20. Sun XC, Lei Y (2017) Fluorescent carbon dots and their sensing applications. TrAC Trends Anal Chem 89:163–180
21. Yu HJ, Shi R, Zhao YF, Waterhouse GIN, Wu LZ, Tung CH, Zhang TR (2016) Smart utilization of carbon dots in semiconductor photocatalysis. Adv Mater 28:9454–9477
22. Li HT, Sun CH, Ali MT, Zhou FL, Zhang XY, MacFarlane DR (2015) Sulfated carbon quantum dots as efficient visible-light switchable acid catalysts for room-temperature ring-opening reactions. Angew Chem Int Ed 54:8420–8424
23. Choi Y, Kim S, Choi MH, Ryoo SR, Park J, Min DH, Kim BS (2014) Highly biocompatible carbon nanodots for simultaneous bioimaging and targeted photodynamic therapy in vitro and in vivo. Adv Funct Mater 24:5781–5789
24. Ruan SB, Qian J, Shen S, Zhu JH, Jiang XG, He Q, Gao HL (2014) A simple one-step method to prepare fluorescent carbon dots and their potential application in non-invasive glioma imaging. Nanoscale 6:10040–10047
25. Ding CQ, Zhu AW, Tian Y (2014) Functional surface engineering of c-dots for fluorescent biosensing and in vivo bioimaging. Acc Chem Res 47:20–30
26. Loo AH, Sofer Z, Bousa D, Ulbrich P, Bonanni A, Pumera M (2016) Carboxylic carbon quantum dots as a fluorescent sensing platform for DNA detection. ACS Appl Mater Interfaces 8:1951–1957
27. Xie C, Nie B, Zeng LH, Liang FX, Wang MZ, Luo LB, Feng M, Yu YQ, Wu CY, Wu YC, Yu SH (2014) Core-shell heterojunction of silicon nanowire arrays and carbon quantum dots for photovoltaic devices and self-driven photodetectors. ACS Nano 8:4015–4022

28. Jin JJ, Chen C, Li H, Cheng Y, Xu L, Dong B, Song HW, Dai QL (2017) Enhanced performance and photostability of perovskite solar cells by introduction of fluorescent carbon dots. ACS Appl Mater Interfaces 9:14518–14524
29. Feng T, Ai XZ, An GH, Yang PP, Zhao YL (2016) Charge-convertible carbon dots for imaging-guided drug delivery with enhanced in vivo cancer therapeutic efficiency. ACS Nano 10:5587–5587
30. Hua XW, Bao YW, Wee FG (2018) Fluorescent carbon quantum dots with intrinsic nucleolus-targeting capability for nucleolus imaging and enhanced cytosolic and nuclear drug delivery. ACS Appl Mater Interfaces 10:16924–16924
31. Qian ZS, Chai LJ, Huang YY, Tang C, Shen JJ, Chen JR, Feng H (2015) A real-time fluorescent assay for the detection of alkaline phosphatase activity based on carbon quantum dots. Biosens Bioelectron 68:675–680
32. Qu FL, Pei HM, Kong RM, Zhu SY, Xia L (2017) Novel turn-on fluorescent detection of alkaline phosphatase based on green synthesized carbon dots and MnO_2 nanosheets. Talanta 165:136–142
33. Tian T, He Y, Ge YL, Song GW (2017) One-pot synthesis of boron and nitrogen co-doped carbon dots as the fluorescence probe for dopamine based on the redox reaction between Cr(VI) and dopamine. Sensors Actuators B Chem 240:1265–1271
34. Liu ZP, Liu LL, Sun MH, Su XG (2015) A novel and convenient near-infrared fluorescence "turn off-on" nanosensor for detection of glucose and fluoride anions. Biosens Bioelectron 65:145–151
35. Zhang J, He LF, Zhang X, Wang JP, Yang L, Liu BH, Jiang CL, Zhang ZP (2017) Colorimetric and SERS dual-readout for assaying alkaline phosphatase activity by ascorbic acid induced aggregation of ag coated au nanoparticles. Sensors Actuators B Chem 253:839–845
36. Liang MJ, Ren Y, Zhang HJ, Ma YX, Niu XY, Chen XG (2017) One-step synthesis of nitrogen, boron co-doped fluorescent carbon nanoparticles for glucose detection. Luminescence 32:1031–1038
37. Miliutina M, Ejaz SA, Iaroshenko VO, Villinger A, Iqbal J, Langer P (2016) Synthesis of 3,3′-carbonyl-bis(chromones) and their activity as mammalian alkaline phosphatase inhibitors. Org Biomol Chem 14:495–502